Redox Biology 12 (2017) 139–149

Contents lists available at ScienceDirect

Redox Biology

journal homepage: www.elsevier.com/locate/redox

Oxidative stress, metabolomics profiling, and mechanism of local anesthetic induced cell death in yeast

Cory H.T. Boone, Ryan A. Grove, Dana Adamcova, Javier Seravalli, Jiri Adamec*

Department of Biochemistry and Redox Biology Center, University of Nebraska – Lincoln, Lincoln, NE, United States of America

ARTICLE INFO

Keywords:
Local anesthetic toxicity
Oxidative stress
Metabolomics profiling
Apoptotic cell death pathways
Flow cytometry
Mass spectrometry

ABSTRACT

The World Health Organization designates lidocaine as an essential medicine in healthcare, greatly increasing the probability of human exposure. Its use has been associated with ROS generation and neurotoxicity. Physiological and metabolomic alterations, and genetics leading to the clinically observed adverse effects have not been temporally characterized. To study alterations that may lead to these undesirable effects, *Saccharomyces cerevisiae* grown on aerobic carbon sources to stationary phase was assessed over 6 h. Exposure of an LC_{50} dose of lidocaine, increased mitochondrial depolarization and ROS/RNS generation assessed using JC-1, ROS/RNS specific probes, and FACS. Intracellular calcium also increased, assessed by ICP-MS. Measurement of the relative ATP and ADP concentrations indicates an initial 3-fold depletion of ATP suggesting an alteration in the ATP:ADP ratio. At the 6 h time point the lidocaine exposed population contained ATP concentrations roughly 85% that of the negative control suggesting the surviving population adapted its metabolic pathways to, at least partially restore cellular bioenergetics. Metabolite analysis indicates an increase of intermediates in the pentose phosphate pathway, the preparatory phase of glycolysis, and NADPH. Oxidative stress produced by lidocaine exposure targets aconitase decreasing its activity with an observed decrease in isocitrate and an increase citrate. Similarly, increases in α-ketoglutarate, malate, and oxaloacetate imply activation of anaplerotic reactions. Antioxidant molecule glutathione and its precursor amino acids, cysteine and glutamate were greatly increased at later time points. Phosphatidylserine externalization suggestive of early phase apoptosis was also observed. Genetic studies using metacaspase null strains showed resistance to lidocaine induced cell death. These data suggest lidocaine induces perpetual mitochondrial depolarization, ROS/RNS generation along with increased glutathione to combat the oxidative cellular environment, glycolytic to PPP cycling of carbon generating NADPH, obstruction of carbon flow through the TCA cycle, decreased ATP generation, and metacaspase dependent apoptotic cell death.

1. Introduction

Lidocaine is the most widely used local anesthetic and generally considered to be of little or no concern to human health when used at recommended applications and practices [1,2]. However when misused such as, inadvertent vascular injection or repeated injections, toxic concentrations may be reached causing adverse side-effects most commonly related to the central nervous system (CNS) [3]. Lidocaine is on the World Health Organization's List of Essential Medicines as both a local anesthetic and antiarrhythmic medication [4]. The primary, clinically relevant mechanism of action of lidocaine is the blockage of voltage gated sodium channels, inhibiting signal conduction and propagation in neurons and preventing the sensation of pain [5]. Lidocaine has a relatively narrow therapeutic index resulting in toxicity when serum concentrations rise above 5 μg mL^{-1} [2]. Initial toxic reactions are excitatory manifesting as tremors, muscle twitching, shivering, and tonic-clonic convulsions. Generalized CNS depression ensues with potential lethargy, coma, cardiovascular collapse, and respiratory depression [2,6,7]. Epidemiological studies and case reports have linked clinical lidocaine usage with cardiac arrest and neurological deficits including, transient radiating post-operative pain, cauda equina syndrome, and seizure onset [8–12].

Previous studies assessing lidocaine toxicity using rat dorsal root ganglion neurons reported superoxide generation, mitochondrial depolarization, intracellular alkalization, and phosphatidylserine externalization [13]. Characteristically, oxidative stress causes protein carbonylation that frequently reduces protein activity [14–16]. In prior examination of lidocaine toxicity in *S. cerevisiae* we have shown carbonylation to multiple proteins involved in carbohydrate metabolism and general bioenergetics. Most notably there was an increase in

* Corresponding author.
E-mail address: jadamec2@unl.edu (J. Adamec).

http://dx.doi.org/10.1016/j.redox.2017.01.025
Received 22 November 2016; Received in revised form 17 January 2017; Accepted 19 January 2017
Available online 03 February 2017

aconitase and glyderaldehyde-3-phosphate dehydrogenase (GAPDH) carbonylation paralleled by a decrease enzyme activity [16]. We also showed there to be a decrease in Cu-Zn superoxide dismutase [16]; potentially providing an explanation for the increased superoxide generation observed upon lidocaine exposure in rat dorsal root ganglion neurons . Additional studies have implicated protein kinase C (PKC) and heat shock proteins (HSPs) in lidocaine toxicity [17–19].

Major limitations of the majority of these studies is that they were targeted, did not examine the system as a whole, and lacked temporal assessment. In addition, prior examination implicates carbon source as a key factor upon hydrogen peroxide stress in *S. cerevisiae*: reporting altered reproductive capacity, growth rates, and markers of oxidative stress [20]. In order to better understand lidocaine fostered pro-oxidant effects in *S. cerevisiae* and relate experimental findings to potential physiological alterations that occur upon lidocaine toxicity in human cells the non-fermentable carbon sources, glycerol and ethanol were used to force mitochondrial dependence for energy generation. Furthermore, stationary phase *S. cerevisiae* is used as a model of human post-mitotic cells to examine molecular mechanisms of aging and neurodegeneration [21,22]. Therefore, cultures were exposed to lidocaine during stationary phase to closely mimic post-mitotic cells.

Mechanisms leading to lidocaine toxicity are independent of the blockade of sodium channels [23]. Voltage gated sodium channels are absent in *S. cerevisiae*, thus permitting the assessment of alterations independent of its primary action and involved in toxicity. Primary toxicity assays based on physiological parameters and genetic background in the non-pathogenic, eukaryotic organism *S. cerevisiae* provides a simple, cost-effective, and tractable model to assess the toxicity of chemical compounds. The yeast *S. cerevisiae* possesses a number of advantages as an experimental model and presents a valuable system for the investigation of basic biological mechanisms common to fungi, plants, animals, and humans; additionally, it has been a proposed model system for the toxicological evaluation of environmental pollutants, gene-environment (GxE) associations, and human CNS disorders [24–26].

It is essential to further investigate the physiological alterations, preferential use of metabolic pathways, and GxE interactions upon exposure to toxic levels of lidocaine to gain a greater mechanistic understanding of the adverse effects observed upon lidocaine administration. Physiological responses assessed were mitochondrial depolarization, ROS/RNS generation, ionomics (most notably calcium), and phosphatidylserine externalization. Metabolomic alterations demonstrated an increase in pentose phosphate pathway (PPP) intermediates and intermediates in the preparatory phase of glycolysis with increases in NADPH. In addition, there are increases in glutathione and its precursor amino acids, cysteine and glutamate, suggestive of a compensatory mechanism to combat the oxidative cellular environment. Genomic studies were focused on cell death and survival pathways using null metacaspase (YCA1) and autophagy (ATG) mutants. Null YCA1 mutants displayed resistance to lidocaine induced cell death; whereas, those mutants lacking proteins of autophagy displayed no significant change or increased sensitivity towards lidocaine induced cell death.

2. Materials and methods

2.1. Organisms, media, and culture methods

Wild type and knockout BY4741 (MatA his3Δ1 leu2Δ0 met15Δ0 ura3Δ0) strains used were obtained from Thermo Scientific. Culture conditions were composed of 50 mL synthetic glycerol/ethanol liquid media (SGE) containing 0.2% [w/v] complete amino acid supplement (US Biological), 0.67% [w/v] yeast nitrogen base (MP Biomedicals), 2% [w/v] glycerol, and 2% [v/v] ethanol. Two-hundred and fifty mL flasks containing 50 mL SGE were initially inoculated with overnight cultures grown in SGE at 0.2 optical density (OD), approximately 10^7 cells mL^{-1}, as measured by Cary 50 UV-Visible spectrophotometer. A hemocytometer was used to convert OD to cells mL^{-1}. Liquid cultures were incubated at 270 RPM and 30 °C in a rotary shaker with growth measured every hour. After approximately 30 h of growth upon entrance into stationary phase Lidocaine HCl (MP Biomedical), hydrogen peroxide (Fisher Scientific), and vehicle control (water) were added to individual cultures.

2.2. Flow cytometry

Temporal analysis of physiological responses of individual cells to stressor exposure was acquired on a BDFACS Canto II (BD Biosciences, San Jose CA, USA) instrument interfaced with FACS Diva v6.11 software (Becton, Dickinson and Co., Franklin Lakes, NJ, USA) and analyzed using FlowJo v10.2 software (TreeStar Inc., Ashland, OR, USA). Instrument acquisition, data analysis, and reporting was carried out as suggested by the International Society for Analytical Cytology (ISAC) [27]. The flow rate was adjusted for a maximum of 2000 events per second and assessed by a time versus scatter plot to eliminate artifacts caused by poor flow. Optimal signal to noise ratio was attained by setting detection threshold voltages in the forward scatter (FSC) and side scatter (SSC) channels just below that of the lowermost yeast cell signals. For multicolor flow cytometry non-treated (vehicle), non-strained and single stained controls were used to correctly adjust hardware and software compensation values. For each sample 10,000 events were collected, and a FSC versus SSC (FSC/SSC) plot of non-treated, unstained *S. cerevisiae* culture for initial gated population P1, to exclude debris in sample analysis. Non-stained and single stained controls were also used for population gating in sample analysis. Each experiment was performed in biological triplicate on independent days. Time points of 1 h, 2 h, 4 h, and 6 h after addition of stressor were evaluated for cell vitality, mitochondrial membrane potential, cellular oxidative state and ROS production, and features of apoptosis.

2.2.1. Cell vitality

Cell vitality was assessed using FungaLight 5-carboxyfluorescein diacetate, acetoxymethyl ester (CFDA,AM)/Propidium Iodide (PI) Yeast Vitality Kit (Life Technologies) according to the manufacturer's protocol. Protocol and LC_{50} concentrations were reported in previous published manuscript [16]. Briefly, volume of culture equivalent to 10^6 cells was collected and exposed to a range of lidocaine concentrations (5-30 mM), hydrogen peroxide concentrations (1-20 mM), and vehicle control. The aliquots were centrifuged at 10,000×*g* for 1 min, washed two times with sterile PBS, re-suspended in 1 mL of PBS, and transferred to 5 mL polystyrene round-bottom tubes (BD Biosciences). The cell suspension was incubated at room temperature for 20 min protected from light with 2 μM CFDA,AM and 9 μM PI. Only the CFDA,AM (-) and PI (+) cell population, indicating damaged membrane along with absent metabolic activity were considered as non-vital, dead cells. The gates for viable and non-viable populations were set up as per manufacturer's instructions and the International Society for the Advancement of Cytometry (ISAC) using single and double stained heat-killed, vehicle-treated, and non-stained cell populations (Supplementary Fig. 1A). Percentage of population within each quadrant of biological triplicate experiments was exported from FlowJo v10.2 software.

2.2.2. Mitochondrial membrane potential

Mitochondrial membrane potential was assessed using cationic dye Mitoprobe 5′,6,6′-tetrachloro-1,1′,3,3′-tetraethylbenzimidazolcarbocyanine iodide (JC-1, Life Technologies), as previously described [28]. Culture volume corresponding to 10^6 cells was centrifuged at 10,000×*g* for 1 min, washed two times with sterile PBS, re-suspended in 37 °C pre-warmed PBS, and transferred to 5 mL polystyrene round-bottom tubes, acquired, and assessed, similar to the vitality assay. For hardware compensation setup and to confirm JC-1 was responsive to

mitochondrial membrane potential, the mitochondrial membrane potential disrupter, carbonyl cyanide 3-chlorophenylhydrazone (CCCP), was added to vehicle-treated cells and allowed to incubate at 37 °C for 5 min. The JC-1 reagent was added to the experimental and CCCP treated cell suspensions to a final concentration of 2 μM and incubated at 37 °C for 20 min protected from light; followed by washing with PBS before analysis. JC-1 fluoresces green as a monomer and demonstrates potential dependent accumulation in the mitochondria causing J-aggregate formation within polarized mitochondria and red fluorescence. A decrease in J-aggregates produces a red (≈590 nm) to green (≈529 nm) fluorescence emission shift and indicates mitochondrial depolarization. The geometric mean fluorescent intensity in the PE and FITC channels of three independent experiments ± SEM was exported from FlowJo v10.2 software for determination and comparison of red: green ratios.

2.2.3. Cellular oxidative stress and ROS detection

General cellular oxidative state and superoxide was detected using the Total ROS/Superoxide Detection Kit (Enzo Life Sciences Inc., Farmingdale, NY), according to manufacturer's protocol [29,30]. The reagents were used in separate experiments to avoid overlap between fluorescent signals upon FACS assessment. Yeast cultures were exposed to stressors and sample volumes equivalent to 10^6 cells were collected from each experimental culture and centrifuged at 400×*g* for 5 min, washed twice with provided wash buffer, and reconstituted in 500 μL of wash buffer with total ROS detection reagent or superoxide detection reagent at 1 μM final concentration. The cell suspension with detection reagent was allowed to incubate for 30 min at 37 °C protected from light. To assure probes were functioning properly vehicle-treated control cells were incubated with superoxide/ROS inducer, pyocyanin (PCN^-) and ROS inhibitor N-acetyl-L-cysteine (NAC) for 30 min prior to staining with probes. Geometric mean fluorescence intensity in the FITC channel for overall oxidative state and PE channel for superoxide assessment of three independent experiments was exported from FlowJo v10.2 software and vehicle-treated control was used as a baseline. The assay for general ROS detection revealing overall cellular oxidative state was performed using the 488 nm argon laser and 530/30 BP filter and superoxide detection was performed using the same excitation laser and a 585/42 BP filter. Peroxynitrite ($ONOO^-$) and hydroxyl radial ($HO^•$) were detected using the species specific probe, Hydroxyphenyl fluorescein (HPF) according to manufacturer's protocol (Cell Technology Inc., Mountain View, CA, USA) as previously reported [31,32]. Briefly, 10^6 cells were collected, centrifuged and reconstituted in HBSS buffer (10 mM HEPES, 1 mM $MgCl_2$, 2 mM $CaCl_2$, and 2.7 mM glucose). HPF was added to a final concentration of 5 μM and incubated at room temperature for 30 min protected from light. Probe detection was accomplished using the FITC channel (530/30 nm BP) and the geometric mean FITC fluorescence ± SEM of three independent experiments is reported.

2.2.4. Apoptosis: phosphatidylserine externalization and membrane permeability

Phosphatidylserine (PS) externalization and membrane permeability was detected using an annexin-V-FITC reagent (BD Biosciences) and PI, respectively, as previously described [33] with some alterations. Culture volume equaling 10^6 cells was centrifuged at 10,000×*g* for 2 min, washed twice with sorbitol buffer (1.2 M sorbitol, 0.5 mM $MgCl_2$, 35 mM K_2HPO_4, pH 6.8), and gently agitated at 37 °C for 30 min in 10 mL sorbitol buffer containing 15 U of lyticase (Sigma) for cell wall digestion. The spheroplasts were washed twice with 10 mL of binding-sorbitol buffer (1.2 M sorbitol, 10 mM HEPES/NaOH, 140 mM NaCl, 2.5 mM $CaCl_2$, pH 7.4) and re-suspended in 500 μL binding-sorbitol buffer. Five μl of both annexin V-FITC and PI (50 mg mL^{-1} working solution) were added to the cell suspension, gently vortexed, and incubated at room temperature for 15 min protected from light. The spheroplasts were then washed with binding-sorbitol buffer, reconstituted in 1 mL binding-sorbitol buffer, and transferred to 5 mL polystyrene round-bottom tubes. A 488 nm argon laser and a 530/30 BP filter for annexin V-FITC and 585/42 BP filter for PI staining assessment. Experiment was performed in biological triplicate and FlowJo v10.2 software was used for sample fluorescence analysis.

2.3. Calcium detection by ICP-MS

Elemental composition was determined using Agilent 7500 Series ICP-MS instrument and assessed using mixed mode [34]. Wild type BY4741 was grown to stationary phase and stressed with LC_{50} dosages of hydrogen peroxide and lidocaine, as described above. Aliquots from each culture equaling approximately 10^6 cells were collected at 1 h, 2 h, 4 h, and 6 h post stress and pelleted at 2500×*g* for 5 min at 4 °C and washed with 50 mM Tris–HCl pH 7 buffer containing 100 mM NaCl, 5 mM EDTA, and protease inhibitor cocktail (Thermo Scientific). To ensure the washes did not add any ion contamination an empty Eppendorf tube was used as mock sample. The cell pellets were completely dried using a speed vac centrifuge. The whole cell pellets were then reconstituted in 200 μL ICP-MS grade concentrated nitric acid spiked with 50 ppb Gallium as an internal standard and incubated for 1 h at 85 °C and then at room temperature for 4 h. The samples were then diluted 20-fold with 50 ppb Gallium in 1% nitric acid so the final concentration of nitric acid was 5% (v/v) [34]. ICP-MS was performed in biological triplicates. The SEM of all Gallium intensities, was within 5% of the average: with 9 out of the 12 triplicates being ≤1% difference from the average. All ions detected were normalized to Gallium and then to phosphate to compensate for small differences in cell density. In addition, phosphate normalization has been used in cisplatin sensitivity and DNA concentration was shown to be the most accurate normalization biomolecule in metabolomics studies [35,36]. Raw data was exported and analyzed using Microsoft excel and SigmaPlot 12.0, and is reported as fold change compared to vehicle-treated control.

2.4. Metabolomics: isolation and detection by MS/MS

Metabolites were isolated using a modified Folch extraction method [37,38]. A volume equivalent to 5 ODs was centrifuged at 1,500×*g* for 1 min at 4 °C, washed once with sterile water, and resuspended in 200 μL of methanol. Approximately, 100 μL of acid washed glass beads were added to the cell suspension and vortexed on high for 1 min and then placed on ice for 30 s; this was repeated a total of three times. The suspension containing cellular debris and glass beads was centrifuged again at 4 °C at 15,000×*g* for 5 min. The metabolite containing supernatant was transferred to a new Eppendorf tube and 400 μL chloroform and 100 μL 5 M NaCl was added. The resulting suspension was vortexed and centrifuged at 1500×*g* in a table top centrifuge for 5 min. Two-hundred μL of the aqueous phase was collected, transferred to a new Eppendorf tube, and dried down in a speed vac. The sample pellets were then resuspended in 50 μL of LC-grade water and injected onto a 4.6×100 mm Amide X-Bridge (3.5 um, Waters, Milford MA) running at 0.5 mL/min. The gradient consisted of 20 mM Ammonium Acetate, 20 mM Ammonium Hydroxide pH=9.0 (A), and LC-grade acetonitrile (B). The gradient was as follows: 2 min hold after injection at 95% B, followed by a 20 min linear gradient from 95% to 5% B, followed by a 5 min hold at 5% B, and final re-equilibration for min at 95% B. The ESI Ion-Source was operated at 500 °C, source gasses 1 and 2 at 70 L/min and electrospray potential at 5000 V and -4200 V in positive and negative modes, respectively. The data was collected in positive and negative ion modes with separate injections of 5 μL and 15 μL, respectively. The mass spectrometer was a triple quadrupole 4000 Q-trap (Sciex, Framingham, MA) operating in MRM analysis mode [39] with a dwell time of 10 ms per transition. Analysis of the chromatograms was performed using MetaboAnalyst 3.0, and

Microsoft Excel was used for statistical analysis, and Sigmaplot 12.0 (Supplementary Table 1) [40] for plotting . All time point samples were analyzed as biological triplicates.

2.5. Cell death and survival pathway assessment

Initial screens of knockout mutant sensitivity towards stressors was assessed in a 96 well plate using PI uptake as the sole indicator of sensitivity. The cells were grown in SGE media to early stationary phase, stressed for 6 h, volume equal to 1 OD was centrifuged at 10,000×*g* for 1 min, reconstituted in 1 mL SGE media, and 200 µL was added to 96 well plate with PI at a final concentration of 9 µM. Uptake of PI, DNA intercalation, and fluorescence was assayed using BioTek Synergy H1 Hybrid Reader for an additional 30 min. Knockout strains that displayed differences in sensitivity compared to wild-type were further explored along with wild-type for comparison. Aliquots equaling 1 OD were centrifuged at 10,000×*g* for 1 min, washed two times in sterile water, serially diluted, and spot plated onto SGE and SD agar plates.

3. Results and discussion

3.1. Toxicity study

The toxicity study and the concentrations used are the same as used for proteomics studies in prior published manuscript [16]. In order to compare physiological responses, metabolomics, and genomics involved in cell malfunction and death it was necessary to establish comparable toxic concentrations; thus, the initial set of experiments was constructing dose response curves to varying concentrations of hydrogen peroxide and lidocaine. Upon exposure to each stressing agent, aliquots from each culture were collected at 1 h, 2 h, 4 h, and 6 h, post exposure and treated with CFDA,AM and PI. Forward scatter versus side scatter plot (FSC/SSC) was used to select a population gate (P1) of cells that were similar in size and morphology to prevent potential contaminating debris in the samples (Supplementary Fig. 1B). Cell populations that were CFDA,AM positive (Q2 and Q3 of Supplementary Fig. 1C) were considered vital regardless of PI staining because of previous reports suggesting that upon stress vital yeast cells may become transiently permeable for up to 4 h and CFDA,AM staining alone correctly predicts the minimum inhibitory concentration of multiple antifungal agents [41,42]. The non-vital population stained CFDA,AM (-) and PI (+) and is the upper left quadrant (Q1) in Supplementary Fig. 1C. Concentrations that caused 50% cell death at 6 h following agent exposure were 20 mM hydrogen peroxide and 30 mM lidocaine. The mean percent cell death of three independent experiments ± SEM Is reported in Supplementary Fig. 1D and displayed Fig. 1A. Representative 5% contour dot plots are shown in Supplementary Fig. 1E. The concentrations of stressors used for all subsequent experiments were the determined LC_{50} at 6 h post exposure: 20 mM hydrogen peroxide and 30 mM lidocaine. Concentrations of hydrogen peroxide are consistent with the literature that has reported stationary phase yeast grown on aerobic carbon source(s) are more resistant to pro-oxidants than logarithmic phase cultures grown on fermentable carbon sources [20,43–45]. Although the exact mechanism of this phenomenon is still unclear it may be related to the alternation in transport/permeability, changes in enzymatic activities or very probably by combination of several factors [46–48].

3.2. Mitochondrial depolarization remains consistent with lidocaine exposure

Mitochondrial membrane potential (MMP) depolarization is a characteristic feature in early stage apoptosis [49]. To assess the effects of stressor exposure on MMP, cells were treated with an LC_{50} dose of hydrogen peroxide and lidocaine. Samples were taken temporally at 1 h, 2 h, 4 h, and 6 h post exposure, stained with JC-1, measured by FACS and assessed, as described in materials and methods. Population gating was initially performed using FSC/SSC plot (Supplementary Fig. 2A); the P1 region includes events of the appropriate size and scatter for yeast cells and was used to exclude debris in sample analysis. The P1 population was further gated using a negative vehicle-treated control and (+) CCCP control (Supplementary Fig. 2B). Population labeled P2 in Supplementary Fig. 2B represents cells with polarized mitochondria; whereas, population labeled P3 represents cells with depolarized mitochondria. Upon JC-1 staining polarized mitochondria are marked by JC-1 aggregate formation and orange-red fluorescence; whereas, depolarized mitochondria are marked by JC-1 monomer formation and green fluorescence. Thus, mitochondrial depolarization is signified by a decrease in the red to green fluorescence ratio [50]. The vehicle-treated and CCCP treated controls displayed a mean PE to FITC ± SEM ratio of all replicates of 13.74 ± 1.03, and 0.47 ± 0.06, respectively throughout the time course. The geometric mean fluorescence intensity in the PE and FITC channels of three independent experiments was exported from FlowJo v10.2 software and the PE to FITC ratio (red: green) ± SEM (Supplementary Fig. 2C) was used to assess stressor induced temporal mitochondrial membrane depolarization as percent of vehicle-treated control ratios (Fig. 1B). Representative dot plots display temporal mitochondrial depolarization induced by exposure to an LC_{50} dose throughout the 6 h time course of hydrogen peroxide and lidocaine (Supplementary Fig. 2D).

Membrane potentials across mitochondria within a single cell display intracellular heterogeneity [51]. A distinct advantage of JC-1

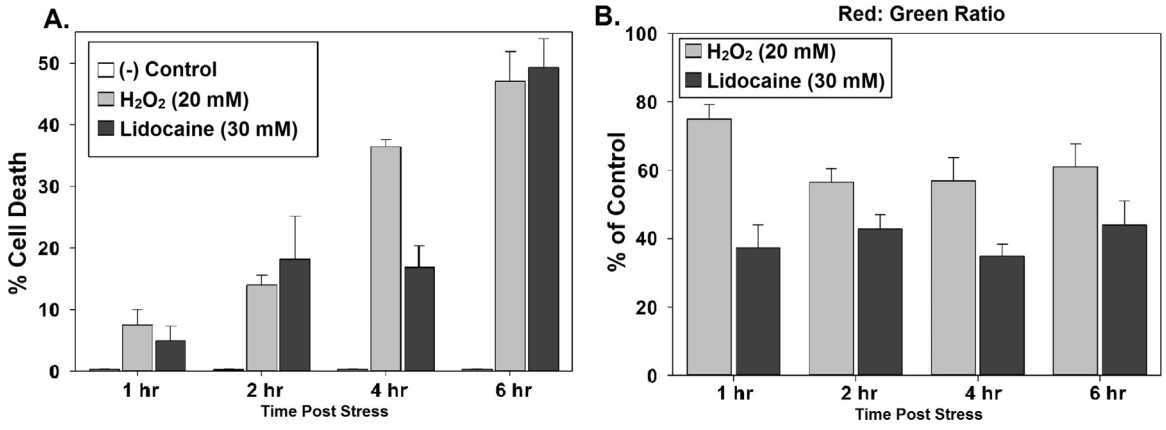

Fig. 1. Xenobiotic Induced Cell Death and Mitochondrial Depolarization: A. Bar graph representing the mean percentage non-vital cells (Q1) ± SEM of three independent experiments; B. Bar graphs representing the mean ratio of red (J-aggregates) to green (J-monomers) ± SEM of three independent experiments normalized to the negative control.

in assessing MMP is that it produces both quantitative, considering the pure fluorescence intensity displayed as a ratio (Fig. 1B), and qualitative, shown as the shift from green to orange (or red) fluorescence emission shown in the dot plots (Supplementary Fig. 2D). Therefore, the bar graphs shown in Fig. 1B define the difference in red to green fluorescence representing overall MMP depolarization within the population; whereas, the dot plots illustrate the shift from green to orange fluorescence descriptive of mitochondrial depolarization heterogeneity within the same cell. Six hour temporal quantitative assessment of LC_{50} dose of hydrogen peroxide suggests that MMP is slightly decreased to approximately 75% that of the negative control at 1 h post stress and continues to decrease to approximately 60% that of the negative control at further time points assessed. An LC_{50} dose of lidocaine shows a consistent decrease in MMP of approximately 40% of control throughout the time course (Fig. 1B). Six hour temporal qualitative assessment of LC_{50} dose of hydrogen peroxide shows that at 1 h post stress very few cells display complete mitochondrial depolarization compared to the negative control (≈ 6.5%) and the percentage of cells increases (P3 population) at 2 (≈ 18%) and 4 (≈26%) h post stress, but decreases at 6 h (≈ 13%) post stress (Supplementary Fig. 2D). Compared to hydrogen peroxide, an LC_{50} dose of lidocaine displays a roughly consistent percentage of cells with complete MMP depolarization throughout the time course, roughly 19%, 25%, 26%, and 21% at 1 h, 2 h, 4 h, and 6 h post exposure, respectively (Supplementary Fig. 2D). Lidocaine induced total cellular mitochondrial depolarization in 20–25% of the population consistently throughout the time course. Merging the quantitative results (red: green ratio) with the qualitative results (dot plots) suggests that hydrogen peroxide induces MMP depolarization at initial and later time points in a more heterogeneous manner than lidocaine.

3.3. ROS/RNS formation remains persistent with lidocaine exposure

The formation of reactive oxygen species (ROS) and their involvement in apoptosis in yeast has been established [52]. ROS levels were assessed using probes specific for certain oxidative species using FACS. Each probe was assessed in three independent experiments and the geometric mean exported from FlowJo v10.2 software for statistical analysis. Cellular oxidative state was measured by assessing general ROS levels using a cell permeable probe reactive with hydrogen peroxide (H_2O_2), peroxynitrite ($ONOO^-$), hydroxyl radial ($HO^\bullet$), nitric oxide (NO), and peroxyl radical ($ROO^\bullet$) fluorescent in the 530 nm (FITC) channel (ENZO Life Sciences) [29,30]. Population (P1) measured was gated using a FSC/SSC plot (Supplementary Fig. 3A). Vehicle-treated control was incubated with Pyocyanin (PCN^-) and N-acetyl-L-cysteine (NAC) for a positive and negative control of probe reactivity towards ROS generation, respectively (Supplementary Fig. 3B). Fluorescence in the FITC channels was assessed by exporting the geometric mean fluorescence and statistically analyzed using SigmaPlot 12.0 (Supplementary Fig. 3C). The geometric mean of the vehicle-treated control was 270.50 ± 7.91 throughout the time course. The initial general oxidative state of the cell was highest upon 20 mM hydrogen peroxide exposure with an approximate 4.5-fold increase, in contrast to a 3-fold increase upon 30 mM lidocaine exposure, compared to vehicle-treated control at the 1 h time point (Fig. 2A). Cellular oxidative state continued to rise at the 2 h time point for all both hydrogen peroxide and lidocaine (Fig. 2A). Hydrogen peroxide and lidocaine exposure caused a continuing increase in cellular oxidative state throughout the time course with roughly a 10-fold and 5-fold increase at the 6 h time point, respectively (Fig. 2A). Representative offset histograms of general cellular oxidative state upon exposure to hydrogen peroxide and lidocaine, and vehicle treated control at each time point measured are displayed in Supplementary Fig. 3D.

To assess the generation of superoxide, a superoxide specific probe (Enzo Life Sciences) [29,30] fluorescent in the 585 nm (PE) channel indicated a significant increase in lidocaine induced superoxide levels compared to hydrogen peroxide exposed yeast cultures. A FSC/SSC plot was used to set up a gate to assess population (P1) of interest (Supplementary Fig. 4A). The fluorescent geometric mean PE ± SEM of three independent experiments was exported from FlowJo v10.2 software for analysis. The vehicle-treated, PCN^-, and NAC treated controls had geometric mean PE fluorescence of 115.98 ± 4.21, 4691 ± 525, and 83.03 ± 4.28, respectively. Representative overlaid histograms show a decreased PE fluorescence with NAC treatment and an increase in PE fluorescence compared to vehicle-treated control (Supplementary Fig. 4B). Hydrogen peroxide treatment caused an initial and constant increase in superoxide production of approximately 2-fold that continued throughout the entire time course (Fig. 2B). Lidocaine caused a rapid and consistent increase in superoxide production with approximate increases compared to the negative control of 4-fold, 6-fold, 8-fold, and 13-fold at 1 h, 2 h, 4 h, and 6 h post stress, respectively (Fig. 2B). Representative offset histograms for all time points and treatments displayed in Supplementary Fig. 4D.

To further explore the differences in reactive oxygen species production upon exposure to the aforementioned stressors, HPF was used to assess hydroxyl radical and peroxynitirite generation [31,32]. As above, a FSC/SSC plot was used to gate population (P1) of interest to exclude debris during measurement and analysis (Supplementary Fig. 5A). Pyocyanin and NAC were also used as a positive and negative controls, respectively. A left shift, decrease in HPF fluorescence was observed with incubation of NAC, and an increase in HPF fluorescence, or right shift of the analyzed histograms was noted upon PCN^- incubation (Supplementary Fig. 5B). The FITC geometric mean fluorescence of three independent experiments was exported and analyzed, as described (Supplementary Fig. 5C). Upon HPF incubation the vehicle-treated control exhibited a mean ± SEM of 158.83 ± 10.54. While, the PCN and NAC incubated samples displayed a mean fluorescence of 2825 ± 131, and 110.67 ± 1.20, respectively; illustrated in Supplementary Fig. 5B. Hydroxyl radical and peroxynitrite assessed was similar in pattern to the oxidative state of the cell assessed above. With both stressors having an approximate 2-fold increase in geometric mean compared to control at the 1 h time point (Fig. 2C). Likewise, hydrogen peroxide exposure caused the most rapid increase in hydroxyl radical and peroxynitrite formation reaching a maximum of 6-fold at the 6 h time point (Fig. 2C). Lidocaine also displayed a persistent increase in hydroxyl radical and peroxynitrite formation throughout the time course with a maximum value of 3-fold at 6 h post exposure (Fig. 2C). Offset histograms are also representing the observed shifts in HPF fluorescence and hydroxyl radical and peroxynitrite formation (Supplementary Fig. 5D). Vertical axis is the cell count, while the horizontal axis is HPF fluorsescence, with a right shift signifying greater fluorescence and hydroxyl radical and peroxynitrite formation.

3.4. Lidocaine increased intracellular calcium concentrations

Cytosolic calcium may increase as a result of being released by intracellular storage of the mitochondria or endoplasmic reticulum. Alternatively, cytosolic calcium may also increase due to increased membrane permeability or uptake of extracellular calcium. ICP-MS was performed on whole cells; thus, the increased cellular calcium suggests increased uptake of extracellular calcium upon lidocaine exposure. Ionic levels were first normalized using Gallium as an internal standard, and then calcium levels were normalized using phosphate. Lidocaine initially induced a 2 to 3-fold increase at the 1 and 2 h time points with a maximum of approximately 5-fold increase in intracellular calcium at the 4 and 6 h time points (Fig. 2D). Hydrogen peroxide induced a maximum intracellular calcium of approximately 1.5-fold increase compared to the negative control (Fig. 2D). Previous studies reporting a link between increased intracellular calcium and cellular alkalization, and lidocaine induced intracellular alkalization support these data [13,53].

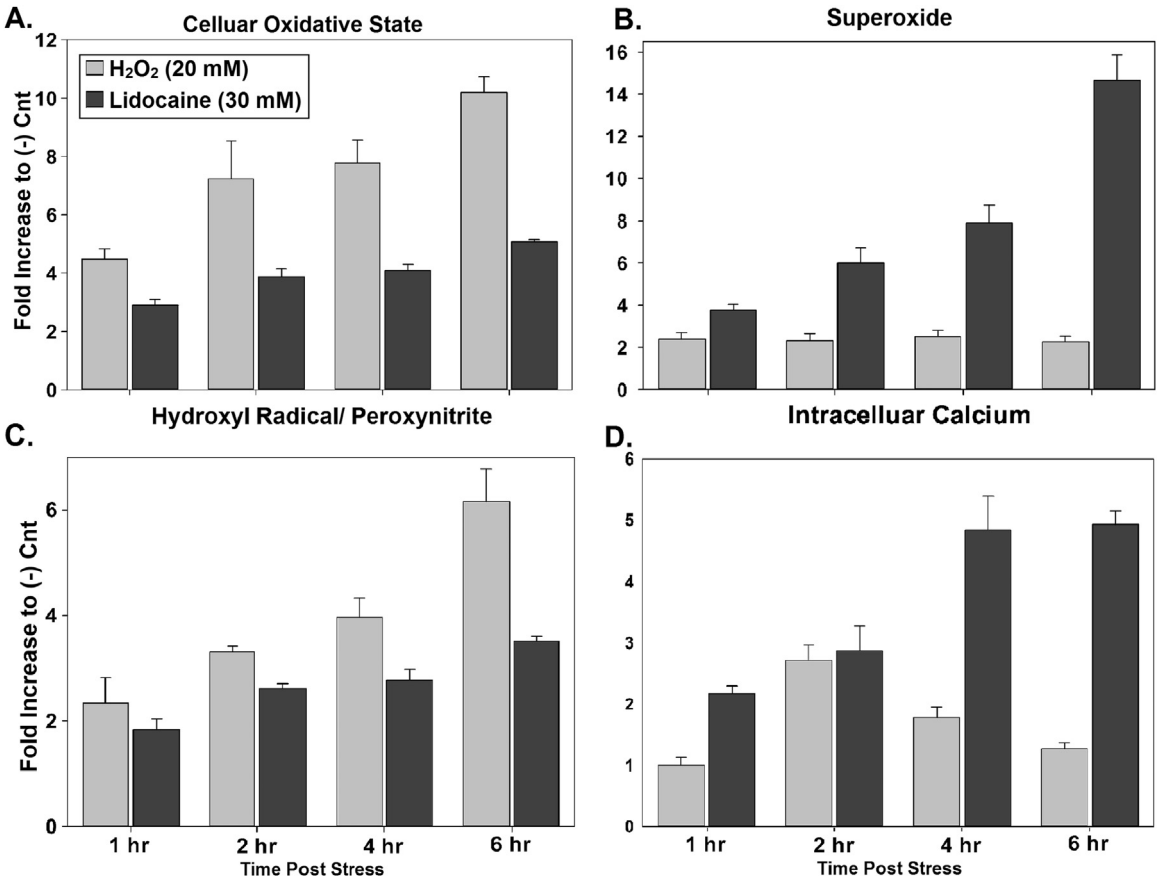

Fig. 2. Xenobiotic Induced Oxidative Stress and Intracellular Calcium Accumulation: A.-C. : Assessed using general and species specific ROS/RNS probes and FACS; A. Cellular oxidative environment, bar graphs representing the geometric mean fluorescence intensity measured in the FITC channel ± SEM of three independent experiments; B. Superoxide generation, bar graphs representing the FlowJo exported geometric mean fluorescence intensity measured in the PE channel ± SEM of three independent experiments; C. Hydroxyl radial and peroxynitrite generation, bar graphs representing the geometric mean fluorescence intensity in the FITC channel ± SEM of three independent experiments of HPF fluorescence; D. Intracellular calcium measured in WCL. Performed using ICP-MS. First normalized to internal standard Ga, then normalized to phosphate levels for cell density.

3.5. Metabolic profiling: lidocaine induces ATP depletion, carbon cycling toward PPP, and glutathione biosynthesis

A total of 255 metabolites were profiled in positive and negative modes by our LC-MS/MS analysis method [39]. The majority of the metabolites reported had a standard error of mean within 15% of the mean (Table 1). Both hydrogen peroxide and lidocaine had a trend to initially decrease ATP compared to the negative control (Table 1 and Fig. 3). In addition, ADP was increased approximately 2-fold upon hydrogen peroxide and lidocaine exposure. The direct ratio of ATP to ADP cannot be deduced due to the methodology used. However, the substantial decrease in ATP, along with the substantial increase in ADP in the first 4 h of xenobiotic exposure compared to the negative control would be indicative of a decrease in the ATP:ADP ratio upon initial stress. At 6 h post stress both the ATP and ADP levels are not significantly different from the negative control, suggesting that after 6 h of exposure to both hydrogen peroxide and lidocaine the surviving population has recovered to the energetic status approximately equivalent to that of non-treatment cells. Similar correlation can be drawn for NAD+ and NADH ratios, as lidocaine exposure initially induced a roughly 2-fold decrease in NADH and 2-fold increase in NAD+. At 6 h post exposure, the NADH and NAD+ concentrations were approximately 80% and 130% of the negative control, respectively indicating a substantial recovery in the NADH: NAD+ ratio (Table 1 and Fig. 3).

The overall decrease in cellular energy status in the initial 4 h for hydrogen peroxide and lidocaine exposure may be explained by the general inhibition of glycolysis. Previous experiments have reported lidocaine induced oxidative modification to GAPDH with diminished activity [16]. Similarly, metabolite analysis displayed an initial 5-fold, 2-fold, and 2-fold decrease in PEP, pyruvate, and alanine, respectively; which is indicative of a decrease in glycolysis [54,55]. Pyruvate concentrations recovered to approximately 85% that of the negative control after 6 h lidocaine exposure (Table 1 and Fig. 3). In addition, there was an approximate initial 5-fold increase in fructose-6-phosphate (F6P), fructose-1,6-bisphosphate (F16BP), dihydroxyacetone phosphate (DHAP), and glyceraldehyde-3-phosphate (GAP), most notably with lidocaine exposure (Fig. 3). DHAP remained elevated at similar levels throughout the time course; while, other metabolites in the preparatory phase of glycolysis that connect the PPP with glycolysis decreased throughout the time course, but were still approximately 2- to 3-fold that of the negative control at 6 h exposure point (Table 1 and Fig. 3). These metabolites are upstream of GAPDH and would be expected to accumulate upon a decrease in its activity. Likewise, TCA cycle enzyme ACON oxidation caused a 3-fold to 2-fold increase in citrate and decrease in isocitrate. Alpha-ketoglutarate (α-KG), malate (Mal), and oxaloacetate (OAA) were initially elevated 3- to 6-fold upon lidocaine exposure (Table 1 and Fig. 3). Suggestive that anaplerotic reactions, such as OAA and glutamate conversion to α-KG and aspartate were initiated in an attempt to maintain NADH levels required for sufficient oxidative phosphorylation and energy generation [56].

Initial inhibition of glycolysis redirects the carbon flow through the parallel and competing PPP with an initial increase between 3-fold to 5-fold of D-6-phospho-glucono-δ-lactone (6PGL), 6-phospho-gluconate (6PG), seduheptulose-7-phosphate (S7P), and erythrose-4-phosphate (E4P) compared to the negative control. An approximate 2-fold

Table 1
Metabolite Fold Change to Negative Control: Fold change to negative control for hydrogen peroxide and lidocaine exposure reported as mean ± SEM for three independent experiments. p value reported for hydrogen peroxide (H) to lidocaine (L) and for each stress compared to negative control (C). Glucose-6-phosphate (G6P), fructose-6-phosphate (F6P), fructose-1,6-bisphosphate (F16BP), dihydroxyacetone phosphate (DHAP), glyceraldehyde-3-phosphate (GAP), phosphyenolpyruvate (PEP), pyruvate (Pyr), alanine (Ala), citrate (Cit), isocitrate (IsoCit), Alpha-ketoglutarate (α-KG), malate (Mal), oxaloacetate (OAA), D-6-phospho-glucono-δ-lactone (6PGL), 6-phosphogluconate (6PG), seduheptulose-7-phosphate (S7P), and erythrose-4-phosphate (E4P).

Metabolite	Hour	H_2O_2 (Fold Change)	Lidocaine (Fold Change)	p value		
Glycolysis				C vs. H	C vs. L	H vs. L
F6P	1	1.70 ± 0.07	5.67 ± 0.17	0.0048	0.0001	0.0003
	2	4.15 ± 1.66	5.09 ± 0.76	0.0366	0.0629	0.0715
	4	1.76 ± 0.03	2.59 ± 0.13	0.0003	0.0086	0.0335
	6	1.36 ± 0.05	2.11 ± 0.13	0.0138	0.0098	0.0216
F16BP	1	2.20 ± 0.13	4.79 ± 0.24	0.0393	0.0011	0.0042
	2	1.95 ± 0.14	3.46 ± 0.19	0.0040	0.0004	0.0046
	4	1.92 ± 0.27	3.25 ± 0.29	0.0215	0.0545	0.1633
	6	2.56 ± 0.18	2.68 ± 0.38	0.0450	0.0088	0.0013
GAP	1	2.03 ± 0.01	5.11 ± 0.12	0.0005	0.0007	0.0013
	2	2.16 ± 0.05	5.26 ± 0.08	0.0016	0.0002	0.0001
	4	1.66 ± 0.07	3.10 ± 0.05	0.0088	0.0010	0.0059
	6	1.45 ± 0.15	3.10 ± 0.20	0.1012	0.0079	0.0314
DHAP	1	1.82 ± 0.05	12.32 ± 0.60	0.0019	0.0013	0.0017
	2	2.02 ± 0.04	9.10 ± 0.22	0.0013	0.0002	0.0005
	4	2.03 ± 0.10	5.89 ± 0.10	0.0075	0.0001	0.0003
	6	1.84 ± 0.10	6.04 ± 0.15	0.0165	0.0006	0.0014
PEP	1	-2.42 ± 0.06	-5.26 ± 0.01	0.0152	0.0038	0.0458
	2	-2.98 ± 0.01	-2.44 ± 0.02	0.0067	0.0088	0.0002
	4	-2.20 ± 0.45	-1.90 ± 0.03	0.0113	0.0076	0.0692
	6	-1.60 ± 0.05	-1.39 ± 0.04	0.0308	0.0330	0.0686
Pyr	1	-2.79 ± 0.03	-1.83 ± 0.03	0.0009	0.0054	0.0457
	2	-2.66 ± 0.03	-1.85 ± 0.03	0.0011	0.0048	0.0780
	4	-1.57 ± 0.07	-1.56 ± 0.06	0.0479	0.0372	0.8381
	6	1.02 ± 0.13	-1.25 ± 0.06	0.5141	0.1109	0.2131
Acetyl-CoA	1	-1.49 ± 0.03	-4.66 ± 0.02	0.0111	0.0011	0.0005
	2	-1.71 ± 0.04	-4.02 ± 0.03	0.0029	0.0013	0.0092
	4	-1.69 ± 0.10	-1.53 ± 0.05	0.0802	0.0149	0.6795
	6	-1.11 ± 0.08	-1.24 ± 0.05	0.3159	0.0507	0.2650
Pentose Phosphate Pathway						
6PGL	1	3.19 ± 0.27	4.23 ± 0.36	0.0149	0.0065	0.1009
	2	2.52 ± 0.04	2.62 ± 0.19	0.0020	0.0184	0.6678
	4	1.60 ± 0.11	2.19 ± 0.09	0.0195	0.0034	0.0349
	6	1.47 ± 0.09	1.99 ± 0.05	0.0214	0.0023	0.0197
6PG	1	2.02 ± 0.33	3.55 ± 0.53	0.0307	0.0068	0.0038
	2	2.16 ± 0.28	2.73 ± 0.18	0.0129	0.0026	0.0707
	4	1.49 ± 0.10	2.23 ± 0.40	0.0210	0.0362	0.1194
	6	1.31 ± 0.20	1.91 ± 0.06	0.2931	0.0208	0.1781
E4P	1	3.28 ± 0.25	3.48 ± 0.41	0.0065	0.0180	0.5992
	2	2.09 ± 0.26	4.36 ± 0.52	0.0407	0.0182	0.0154
	4	1.42 ± 0.17	3.77 ± 0.05	0.1139	0.0020	0.0127
	6	1.32 ± 0.10	3.63 ± 0.21	0.0853	0.0083	0.0057
S7P	1	1.51 ± 0.62	2.47 ± 0.14	0.5414	0.0011	0.2409
	2	1.81 ± 0.28	2.77 ± 0.34	0.0704	0.0137	0.0043
	4	2.03 ± 0.23	3.96 ± 0.30	0.0464	0.0102	0.0159
	6	2.29 0.23	6.54 ± 0.69	0.0152	0.0131	0.0167
TCA Cycle						
OAA	1	2.00 ± 0.45	1.94 ± 0.04	0.0627	0.2293	0.5305
	2	1.98 ± 0.16	1.78 ± 0.02	0.2270	0.1836	0.4460
	4	1.38 ± 0.19	1.20 ± 0.09	0.3717	0.0267	0.4471
	6	-1.29 ± 0.07	1.01 ± 0.05	0.0171	0.6537	0.0183
Cit	1	1.33 ± 0.09	2.54 ± 0.26	0.0482	0.0026	0.0009
	2	1.28 ± 0.09	2.02 ± 0.20	0.0865	0.0279	0.0559
	4	1.20 ± 0.07	1.40 ± 0.13	0.0759	0.0903	0.2003
	6	1.22 ± 0.17	1.29 ± 0.05	0.3340	0.1684	0.9747
IsoCit	1	-2.09 ± 0.02	-1.78 ± 0.03	0.0136	0.0132	0.0535
	2	-1.29 ± 0.11	-2.00 ± 0.11	0.2085	0.1281	0.1077
	4	1.04 ± 0.16	-1.16 ± 0.07	0.9805	0.1753	0.3642
	6	1.18 ± 0.23	-1.24 ± 0.05	0.5264	0.0765	0.2050
α-KG	1	1.61 ± 0.13	3.37 ± 0.85	0.0123	0.0200	0.0381
	2	2.01 ± 0.32	3.20 ± 0.30	0.0405	0.0192	0.0433
	4	1.40 ± 0.10	3.12 ± 0.40	0.0732	0.0307	0.0709
	6	1.05 ± 0.05	1.80 ± 0.35	0.5524	0.0440	0.0439
Mal	1	4.50 ± 0.33	6.67 ± 1.51	0.0098	0.0713	0.3746
	2	2.17 ± 0.57	9.75 ± 1.29	0.2245	0.0159	0.0057
	4	1.55 ± 0.59	5.93 ± 1.05	0.4640	0.0073	0.0004
	6	1.42 ± 0.46	6.62 ± 1.72	0.5245	0.0477	0.0219
Amino Acid Metabolism/Antioxidants						
Ala	1	-2.97 ± 0.02	-1.87 ± 0.03	0.0056	0.0131	0.0010
	2	-1.97 ± 0.04	-1.35 ± 0.15	0.0606	0.2819	0.1856
	4	-1.99 ± 0.05	-1.33 ± 0.08	0.0058	0.0953	0.1669
	6	1.02 ± 0.13	1.13 ± 0.09	0.9518	0.2758	0.4889
Glu	1	2.15 ± 0.21	-1.03 ± 0.08	0.0465	0.6900	0.0702
	2	1.07 ± 0.04	1.03 ± 0.06	0.1551	0.6704	0.1608
	4	4.05 ± 0.54	5.70 ± 0.60	0.0110	0.0311	0.2655
	6	4.11 ± 0.25	7.00 ± 0.44	0.0005	0.0001	0.0002
Asp	1	1.47 ± 0.14	2.55 ± 0.07	0.0757	0.0087	0.0264
	2	1.30 ± 0.16	2.76 ± 0.41	0.2231	0.0330	0.0998
	4	1.20 ± 0.24	2.53 ± 0.50	0.5087	0.1555	0.2326
	6	1.10 ± 0.11	1.66 ± 0.14	0.4499	0.0237	0.0599
Cys	1	1.11 ± 0.07	1.64 ± 0.14	0.2491	0.0337	0.0108
	2	2.65 ± 0.14	3.04 ± 0.08	0.0024	0.0020	0.0479
	4	1.20 ± 0.37	4.03 ± 0.40	0.5932	0.0041	0.0399
	6	2.52 ± 0.11	4.40 ± 0.72	0.0012	0.0274	0.0713
Betaine	1	1.04 ± 0.07	3.92 ± 0.44	0.6052	0.0268	0.0353
	2	3.44 ± 0.60	3.10 ± 1.03	0.0372	0.1972	0.9263
	4	1.21 ± 0.10	5.15 ± 1.25	0.1823	0.0385	0.0447
	6	1.24 ± 0.16	4.98 ± 1.04	0.2306	0.0312	0.0380
Putrescine	1	1.03 ± 0.14	1.17 ± 0.23	0.9586	0.6832	0.3224
	2	-1.32 ± 0.31	1.60 ± 0.47	0.4337	0.3471	0.3068
	4	1.12 ± 0.14	1.88 ± 0.52	0.5877	0.1574	0.1394
	6	1.02 ± 0.13	2.15 ± 6.98	0.6796	0.0186	0.0120
GSH	1	1.29 ± 0.13	-1.09 ± 0.12	0.1529	0.5282	0.0866
	2	1.66 ± 0.24	2.00 ± 0.22	0.1360	0.0647	0.2719
	4	1.62 ± 0.24	9.62 ± 1.54	0.1364	0.0161	0.0277
	6	2.10 ± 0.55	5.31 ± 0.52	0.1027	0.0363	0.0961
Energy/Nicotinamide Molecules						
ATP	1	-1.78 ± 0.07	-2.73 ± 0.13	0.1675	0.1596	0.3567
	2	-1.96 ± 0.11	-3.21 ± 0.05	0.1014	0.0428	0.0968
	4	-1.68 ± 0.60	-1.48 ± 0.14	0.0136	0.1875	0.7275
	6	-1.29 ± 0.11	-1.16 ± 0.13	0.1712	0.3622	0.7652
ADP	1	1.99 ± 0.31	2.17 ± 0.11	0.1338	0.0009	0.8404
	2	1.87 ± 0.10	2.64 ± 0.18	0.0001	0.0420	0.1493
	4	1.53 ± 0.21	2.03 ± 0.13	0.1168	0.0642	0.2726
	6	1.08 ± 0.04	1.04 ± 0.28	0.2091	0.7905	0.6627
NAD+	1	3.42 ± 0.37	2.08 ± 0.27	0.0281	0.0543	0.1767
	2	3.37 ± 0.31	2.18 ± 0.20	0.0066	0.0254	0.0074
	4	-1.10 ± 0.11	1.62 ± 0.36	0.4118	0.1763	0.0468
	6	1.37 ± 0.19	1.30 ± 0.14	0.2085	0.1691	0.8463
NADH	1	-4.64 ± 0.03	-2.23 ± 0.08	0.0063	0.0140	0.1242
	2	-4.04 ± 0.04	-2.31 ± 0.03	0.0221	0.0125	0.1493
	4	-2.17 ± 0.03	-2.30 ± 0.05	0.0724	0.0740	0.3445
	6	-1.19 ± 0.20	-1.21 ± 0.12	0.4602	0.3267	0.9076
NADP+	1	-2.47 ± 0.37	-4.67 ± 0.04	0.0450	0.0208	0.0091
	2	-1.75 ± 0.07	-5.53 ± 0.05	0.0467	0.0183	0.0196
	4	-1.32 ± 0.19	-4.45 ± 0.04	0.3377	0.0356	0.0307
	6	1.07 ± 0.20	-2.49 ± 0.05	0.7934	0.0174	0.0418
NADPH	1	2.53 ± 0.31	3.98 ± 0.76	0.0076	0.0253	0.0541
	2	1.68 ± 0.32	3.96 ± 0.91	0.1167	0.0254	0.0370
	4	1.38 ± 0.07	3.72 ± 0.34	0.0089	0.0363	0.0471
	6	1.23 ± 0.28	3.92 ± 0.49	0.5083	0.0020	0.0055

increase to that of the negative control was observed upon lidocaine exposure at the 6 h time point for PPP intermediates (Table 1 and Fig. 3). The abundance of transketolase (TKL), a central enzyme connecting the PPP with glycolysis was previously found to be increased roughly 2-fold upon lidocaine exposure [16]. This rerouting of carbon and preferential use of the PPP over glycolysis results most often from oxidative stress [57]. However, the PPP is also a major source of metabolites that supply multiple anabolic processes [58]. The major cofactor produced by the oxidative branch of the PPP is NADPH, which plays a central role in the glutaredoxin and thioredoxin

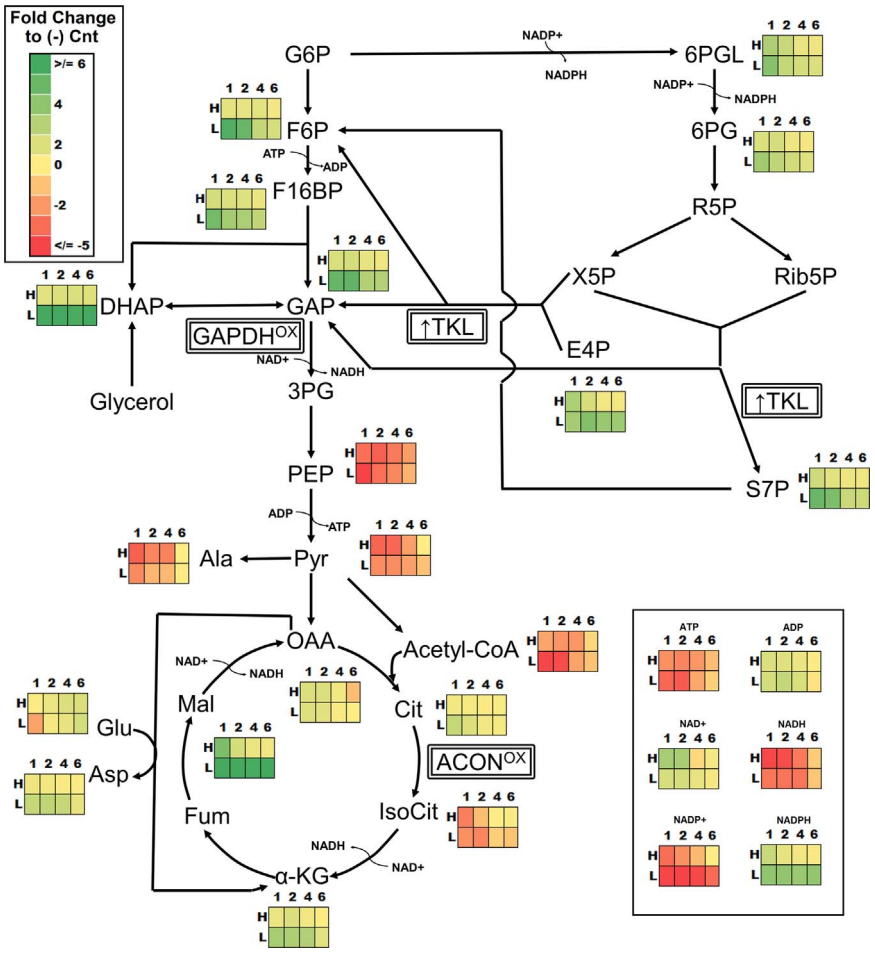

Fig. 3. Temporal assessment of Xenobiotic Induced Alterations in Metabolite Concentrations, Carbohydrate Metabolism Metabolite Pathways and HeatMap: Displayed as fold change to non-treatment negative control. Preferential use of the PPP for NADPH generation. Enzymes shown in boxes were previously reported to be oxidatively modified upon lidocaine exposure with diminished activity (OX) or increased in abundance of transketolase (TKL); see text for citation. Cellular energetics and redox cofactors alterations compared to negative control shown in inset box at bottom right. Color legend with fold change shown in upper left. Glucose-6-phosphate (G6P), fructose-6-phosphate (F6P), fructose-1,6-bisphosphate (F16BP), dihydroxyacetone phosphate (DHAP), glyceraldehyde-3-phosphate (GAP), phosphyenolpyruvate (PEP), pyruvate (Pyr), alanine (Ala), citrate (Cit), isocitrate (IsoCit), Alpha-ketoglutarate (α-KG), malate (Mal), oxaloacetate (OAA), D-6-phospho-glucono-δ-lactone (6PGL), 6-phosphogluconate (6PG), seduheptulose-7-phosphate (S7P), and erythrose-4-phosphate (E4P).

antioxidant systems [59,60]. NADPH and NADP+ levels are altered to a greater extent and time upon lidocaine exposure compared to hydrogen peroxide (Table 1 and Fig. 3). This correlates with greater superoxide production observed upon lidocaine exposure and implies potential redox signaling [61,62]. Following an initial 2-fold decrease in glutathione (GSH) induced by lidocaine, GSH concentrations rose to approximately 2-fold increase compared to the negative control (Table 1). The coordinated increase GSH biosynthetic precursors, glutamate (5- to 7-fold) and cysteine (3- to 5- fold) suggest an increase in the biosynthesis of GSH.

In addition to carbon metabolism, redox homeostasis, and general bioenergetics, additional metabolites that were altered upon stress were betaine and putrescine. Betaine, which is involved in methionine to homocysteine conversion was increased under lidocaine stress throughout the time course at 3 to 4-fold compared to non-stressed control (Table 1). Betaine has been previously reported to be involved in osmotic stress [63]. Putrescine, a polyamine that is a product of arginine and proline catabolism was temporally increased with lidocaine stress reaching its maximum at the 6 h time point at approximately 2-fold increase. Betaine and putrescine were not consistently and significantly altered upon hydrogen peroxide exposure (Table 1). While, polyamines have been reported to be increased upon exposure to alternative stress conditions, this is the first report of altered polyamines, specifically putrescine for lidocaine toxicity.

3.6. Lidocaine causes significant PS externalization

Another hallmark of early apoptosis is loss of plasma membrane asymmetry and phosphatidylserine (PS) externalization. In apoptotic cells PS is translocated from the inner leaflet to the outer leaflet of the plasma membrane; thus exposing PS to the external environment prior to loss of membrane integrity. Annexin V is a calcium dependent PS binding protein [64]. Annexin V conjugated to FITC was used with PI along with FACS to verify the occurrence of apoptosis and membrane permeability. At a single time point this assay does not differentiate between cells that have undergone apoptotic cell death versus an alternative form of cell death because dead cells often stain with both probes. However, over time a population of cells can be followed from Annexin V and PI negative, vital without apoptotic cell death, Annexin V positive and PI negative, early apoptosis with impermeable plasma membranes, and finally to Annexin V and PI positive, end stage apoptosis and cell death. Movement of a population of cells through these three stages is indicative of apoptosis. The intermediate stage of Annexin V positive and PI negative is a vital step to measure as movement of a population from Annexin V and PI negative to Annexin V and PI positive does not indicate PS externalization prior to membrane permeabilization [64].

A SSC/FSC plot was used to select a population (P1) and exclude debris from sample analysis (Supplementary Fig. 6A). A vehicle-

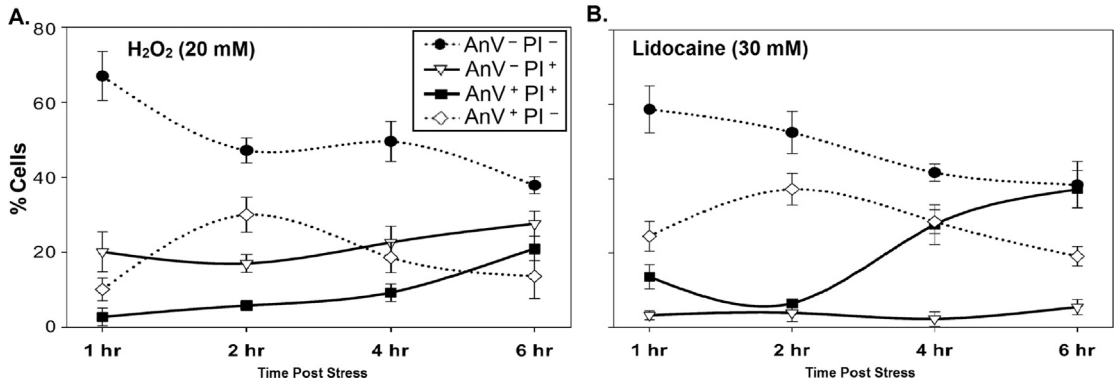

Fig. 4. Line Plots of Temporal Assessment of Phosphatidylserine Externalization Along with Membrane Permeabilization; An Indicating Feature of Apoptosis: A. Hydrogen peroxide; B. Lidociane; . In the line plots for both hydrogen peroxide and lidocaine the AnnexinV- PI- (non-stained) and AnnexinV+ PI- (PS externalization) merge together at similar time points followed by an increase in AnnexinV+ PI+ population. PS externalization occurs prior to membrane permeabilization.

treatment negative control and acetic acid treated apoptosis positive control was used for setting up gates of P1 population (Supplementary Fig. 6B). Line and scatter plots demonstrate population movement through the time course (Fig. 4). The dashed line with filled circles represents Annexin V^- and PI^- population and the dashed line with non-filled diamonds represents Annexin V^+ and PI^- population. For hydrogen peroxide and lidocaine stress the line plots show that a decrease in the Annexin V^- and PI^- population occurs at the same time point as an increase in Annexin V^+ and PI^- population. This is illustrated in Fig. 4A and B as the dashed lines, or filled circle and unfilled diamond converge at the 2 h time point. This temporal assessment is crucial because at 1 h Fig. 4 shows that the filled circle and the unfilled diamond are between 60% and 70% points apart, as denoted by the y-axis; however, at the 2 h time point they are between 20% and 10% points apart (Fig. 4). The lines do not represent measured points; therefore, the lines are an estimation based on the two measured points and the exact movement of the population from 1 h to 2 h is probably not as smooth as the lines represent. However, the line graphs clearly show a temporal decrease between the 1 h and 2 h time points of a population (filled circles) that is annexinV (-) and PI (-) coordinately occurring with a temporal increase of a population (unfilled diamonds) annexinV (+) and PI (-). The subsequent time point then demonstrates a jump in Annexin V^+ and PI^+ population (Fig. 4A and B). This pattern of PS externalization followed by membrane permeabilization is indicative of apoptotic cell death. This is also displayed in the representative %5 probability contour dot plots (Supplementary Fig. 6D) that illustrate hydrogen peroxide induces a relatively consistent temporal uptake of PI (Q1) with PS externalization increasing throughout time course (Q2 and Q3), and lidocaine induces a great deal of PS externalization without PI uptake (Q3) early in the time course while at later points PS externalization is accompanied by PI uptake (Q2) (Supplementary Fig. 6D).

3.7. YCA1, NUC1, and AIF1 null mutants display decreased lidocaine induced cell death

To further verify stressor induced mechanisms of cell death indicated by PS externalization and metabolite analysis, stressor sensitivity of knock out mutants lacking players in various cell death and survival pathways were assessed. Mammalian cells contain multiple caspases with caspase-9 being activated by mitochondrial depolarization and cytochrome C (Intrinsic apoptosis), and caspase-8 being activated by Fas-Associated protein with Death Domain (FADD) receptor (Extrinsic apoptosis). *S. cerevisiae* contains a single known caspase, metacaspase (Yca1). Metacaspase null mutants display significantly reduced susceptibility to hydrogen peroxide and lidocaine induced cell death compared to Wild Type (Fig. 5). Mitochondrial nuclease (Nuc1), a homolog of mammalian endoG, is also released

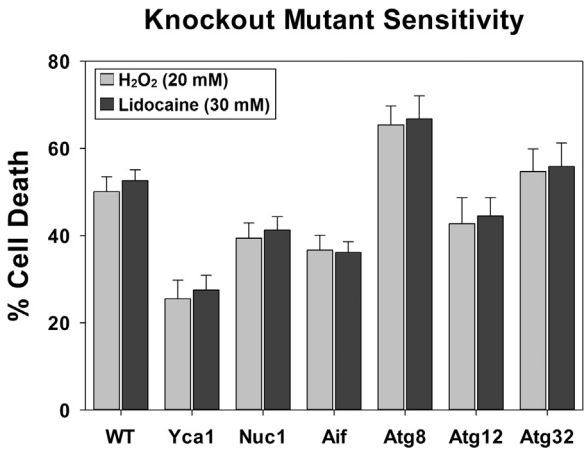

Fig. 5. KO mutant Sensitivity: KO mutants of proteins in pathways of apoptosis (Yca1, Nuc1, Aif) are resistant to hydrogen peroxide and lidocaine, most notably in the Yca1 mutant. KO mutant sensitivity is increased with Atg8, and not altered with Atg12 or Atg32 mutants suggesting that some components of autophagy may play a cytoprotective role.

from permeabilized mitochondria and plays a role in apoptosis through fragmentation of genomic DNA. NUC1 null mutants also display reduced susceptibility to lidocaine induced cell death, although not as profound as Yca1 null mutants. Whereas, KO mutants of autophagy proteins ATG8, ATG12, and ATG32 demonstrated either increased sensitivity or no significant change, suggesting that some components and pathways of autophagy play a cytoprotective role upon lidocaine stress. As outlined by The Nomenclature Committee on Cell Death (NCCD) [65], these data, along with PS externalization indicates lidocaine toxicity and cell death is induced through caspase dependent apoptosis.

4. Concluding remarks

The physiological alterations inducing lidocaine toxicity participate in mitochondrial depolarization, with the excessive generation of ROS/RNS, and intracellular calcium accumulation. Prior reports of oxidative damage accompanied by a decrease in activity of central enzymes of glycolysis (GAPDH) and the TCA cycle (aconitase), along with metabolomics assessment suggests preferential cycling of carbon through the PPP with NADPH generation. It then gets cycled back towards glycolysis through glyceraldehyde-3-phosphate and fructose-6-phosphate. NADPH is a central cofactor in the glutathione and thioredoxin/peroxiredoxin antioxidant systems. The increased NADPH would assist in reducing the oxidative cellular environment [66]. Similarly, the increase in glutathione and its precursors, glutamate and cysteine

suggests that the glutathione system plays an additive role in oxidant detoxification. Alternatively, increased NADPH may increase the electron supply that produces superoxide indicative of redox signaling [61,67]. A general decrease in cellular bioenergetics demonstrated as a decrease in ATP and an increase in ADP upon lidocaine exposure compared to the negative control appears to be the result of oxidation to key enzymes in glycolysis and the TCA cycle that inhibits glycolysis and prevents, or at minimum impedes glycolytic end products from entering the TCA cycle. This is apparent from the decrease in isocitrate, and increase in citrate, α-KG, malate, oxaloacetate, glutamate, and aspartate. The anaplerotic reaction of glutamate to α-KG is essential in maintaining TCA flux and NADH generation for sufficient oxidative phosphorylation in the synthesis of ATP upon lidocaine induced ACON damage. In addition, the accumulation of betaine and calcium implies lidocaine induces an alkaline environment, which has been previously suggested. Finally, the perpetual mitochondrial depolarization, intracellular calcium accumulation, PS externalization, and metacaspase null mutant insensitivity suggests that toxic levels of lidocaine induce cellular demise through caspase dependent apoptotic cell death.

Appendix A. Supplementary material

Supplementary data associated with this article can be found in the online version at http://dx.doi.org/10.1016/j.redox.2017.01.025.

References

[1] P.A. Moore, E.V. Hersh, Local anesthetics: pharmacology and toxicity, Dent. Clin. N. Am. 54 (4) (2010) 587–599.
[2] D.E. Becker, K.L. Reed, Local anesthetics: review of pharmacological considerations, Anesth. Prog. 59 (2) (2012) 90–102.
[3] K. Hampl, T. Steinfeldt, H. Wulf, Spinal anesthesia revisited: toxicity of new and old drugs and compounds, Curr. Opin. Anesthesiol. 27 (5) (2014) 549–555.
[4] World Health Organization. WHO Model List of Essential Medicines 2015. Available from: ⟨http://www.who.int/medicines/publications/essentialmedicines/en/⟩.
[5] A. Scholz, W. Vogel, Tetrodotoxin-resistant action potentials in dorsal root ganglion neurons are blocked by local anesthetics, Pain 89 (1) (2000) 47–52.
[6] R.H. Scholle, J.B. Goetz, J.M. Goodson, P.A. Moore, Life-threatening reactions after pedodontic sedation: an assessment of narcotic, local anesthetic, and antiemetic drug interaction, J. Am. Dent. Assoc. 107 (2) (1983) 239–245.
[7] F. Reynolds, Adverse effects of local anaesthetics, Br. J. Anaesth. 59 (1) (1987) 78–95.
[8] M.M.A. Doumiri, W. Maazouzi, Cardiac arrest after gargling and oral ingestion of 5% lidocaine, Can. J. Anaesth. 55 (2008) 882–883.
[9] G.A. Liguori, V.M. Zayas, Repeated episodes of transient radiating back and leg pain following spinal anesthesia with 1.5% mepivacaine and 2% lidocaine, Reg. Anesth. Pain Med. 23 (5) (1998) 511–515.
[10] M.L. Rigler, K. Drasner, T.C. Krejcie, S.J. Yelich, F.T. Scholnick, J. DeFontes, et al., Cauda equina syndrome after continuous spinal anesthesia, Anesth. Analg. 72 (3) (1991) 275–281.
[11] Y. Auroy, P. Narchi, A. Messiah, L. Litt, B. Rouvier, K. Samii, Serious complications related to regional anesthesia: results of a Prospective Survey in France, Anesthesiology 87 (3) (1997) 479–486.
[12] M. Bensghir, N. Badou, A. Houba, H. Balkhi, C. Haimeur, H. Azendour, Convulsions during cataract surgery under peribulbar anesthsia: a case report, J. Med. Case Rep. 8 (2014) 218–221.
[13] S. Onizuka, T. Yonaha, R. Tamura, M. Kasiwada, T. Shirasaka, I. Tsuneyoshi, Lidocaine depolarizes the mitochondrial membrane potential by intracellular alkalization in rat dorsal root ganglion neurons, J. Anesth. 25 (2) (2011) 229–239.
[14] J.-H. Kim, M. Sedlak, Q. Gao, C.P. Riley, F.E. Regnier, J. Adamec, Oxidative stress studies in yeast with a frataxin mutant: a proteomics perspective, J. Proteome Res. 9 (2) (2009) 730–736.
[15] J.-H. Kim, M. Sedlak, Q. Gao, C.P. Riley, F.E. Regnier, J. Adamec, Dynamics of protein damage in yeast frataxin mutant exposed to oxidative stress, OMICS: J. Integr. Biol. 14 (6) (2010) 689–699.
[16] C.H.T. Boone, R.A. Grove, D. Adamcova, C.P. Braga, J. Adamec, Revealing oxidative damage to enzymes of carbohydrate metabolism in yeast: an integration of 2D DIGE, quantitative proteomics and bioinformatics, Proteomics 16 (13) (2016) 1889–1903.
[17] E.Q. Villarruel, E. Borda, L. Sterin-Borda, B. Orman, Lidocaine-induced apoptosis of gingival fibroblasts: participation of cAMP and PKC activity, Cell Biol. Int. 35 (8) (2011) 783–788.
[18] S.H.F.H. Do, B.M. Ham, Z. Zuo, The effects of lidocaine on the activity of glutamate transporter EAAT3: the role of protein kinase C and phosphatidylinositol 3-kinase, Anesth. Analg. 95 (5) (2002) 1263–1268.
[19] G.A. Senisterra, J.K. Lepock, Thermal Destabilization of Transmembrane Proteins by Local Anaesthetics, Taylor & Francis, London, ROYAUME-UNI, 2000, pp. 1–17.
[20] R. Vasylkovska, N. Petriv, H. Semchyshyn, Carbon sources for yeast growth as a precondition of hydrogen peroxide induced hormetic phenotype, Int. J. Microbiol. 2015 (2015) 697813.
[21] S. Kumar, S.D. Lefevre, M. Veenhuis, I.J. van der Klei, Extension of yeast chronological lifespan by methylamine, PLoS One 7 (11) (2012) e48982.
[22] Q. Chen, Q. Ding, J.N. Keller, The stationary phase model of aging in yeast for the study of oxidative stress and age-related neurodegeneration, Biogerontology 6 (1) (2005) 1–13.
[23] S. Sakura, A.W. Bollen, R. Ciriales, K. Drasner, Local anesthetic neurotoxicity does not result from blockade of voltage-gated sodium channels, Anesth. Analg. 81 (2) (1995) 338–346.
[24] I.C. Ribeiro, I. Veríssimo, L. Moniz, H. Cardoso, M.J. Sousa, A.M.V.M. Soares, et al., Yeasts as a model for assessing the toxicity of the fungicides penconazol, cymoxanil and dichlofluanid, Chemosphere 41 (10) (2000) 1637–16342.
[25] C.M. McHale, M.T. Smith, L. Zhang, Application of toxicogenomic profiling to evaluate effects of benzene and formaldehyde: from yeast to human, Ann. N. Y. Acad. Sci. 1310 (1) (2014) 74–83.
[26] L. Miller-Fleming, F. Giorgini, T.F. Outeiro, Yeast as a model for studying human neurodegenerative disorders, Biotechnol. J. 3 (3) (2008) 325–338.
[27] J.A. Lee, J. Spidlen, K. Boyce, J. Cai, N. Crosbie, M. Dalphin, et al., MIFlowCyt: the minimum information about a flow cytometry experiment, Cytom. Part A: J. Int. Soc. Anal. Cytol. 73 (10) (2008) 926–930.
[28] C.-Y. Lai, E. Jaruga, C. Borghouts, S.M. Jazwinski, A Mutation in the ATP2 gene abrogates the age asymmetry between mother and daughter cells of the yeast *Saccharomyces cerevisiae*, Genetics 162 (1) (2002) 73–87.
[29] H. Kanzaki, F. Shinohara, M. Kajiya, T. Kodama, The Keap1/Nrf2 protein axis plays a role in osteoclast differentiation by regulating intracellular reactive oxygen species signaling, J. Biol. Chem. 288 (32) (2013) 23009–23020.
[30] A. Zhang, P. Wang, X. Ma, X. Yin, J. Li, H. Wang, et al., Mechanisms that lead to the regulation of NLRP3 inflammasome expression and activation in human dental pulp fibroblasts, Mol. Immunol. 66 (2) (2015) 253–262.
[31] W. Paulander, Y. Wang, A. Folkesson, G. Charbon, A. Løbner-Olesen, H. Ingmer, Bactericidal antibiotics increase hydroxyphenyl fluorescein signal by altering cell morphology, PLoS One 9 (3) (2014) e92231.
[32] Setsukinai K-i, Y. Urano, K. Kakinuma, H.J. Majima, T. Nagano, Development of novel fluorescence probes that can reliably detect reactive oxygen species and distinguish specific species, J. Biol. Chem. 278 (5) (2003) 3170–3175.
[33] P.A. de Castro, M. Savoldi, D. Bonatto, M.H. Barros, M.H.S. Goldman, A.A. Berretta, et al., Molecular characterization of propolis-induced cell death in *Saccharomyces cerevisiae*, Eukaryot. Cell 10 (3) (2011) 398–411.
[34] J. Seravalli, Inductively Coupled plasma–mass spectrometry as a tool for high-throughput analysis of plants, in: J. Normanly (Ed.)High-Throughput Phenotyping in Plants: Methods and Protocols, Humana Press, Totowa, NJ, 2012, pp. 269–288.
[35] M. Corte-Rodríguez, M. Espina, L.M. Sierra, E. Blanco, T. Ames, M. Montes-Bayón, et al., Quantitative evaluation of cellular uptake, DNA incorporation and adduct formation in cisplatin sensitive and resistant cell lines: Comparison of different Pt-containing drugs, Biochem. Pharmacol. 98 (1) (2015) 69–77.
[36] L.P. Silva, P.L. Lorenzi, P. Purwaha, V. Yong, D.H. Hawke, J.N. Weinstein, Measurement of DNA concentration as a normalization strategy for metabolomic data from adherent cell lines, Anal. Chem. 85 (20) (2013). http://dx.doi.org/10.1021/ac401559v.
[37] J. Folch, M. Lees, G.H.S. Stanley, A simple method for the isolation and purification of total lipides from animal tissues, J. Biol. Chem. 226 (1) (1957) 497–509.
[38] S.J. Ha, G. Showalter, S. Cai, H. Wang, W.M. Liu, A.A. Cohen-Gadol, et al., Lipidomic analysis of glioblastoma multiforme using mass spectrometry, Anal. Chem. 79 (22) (2007) 8423–8430.
[39] M. Yuan, S.B. Breitkopf, X. Yang, J.M. Asara, A positive/negative ion–switching, targeted mass spectrometry–based metabolomics platform for bodily fluids, cells, and fresh and fixed tissue, Nat. Protoc. 7 (5) (2012) 872–881.
[40] J. Xia, I.V. Sinelnikov, B. Han, D.S. Wishart, MetaboAnalyst 3.0—making metabolomics more meaningful, Nucleic Acids Res. 43 (W1) (2015) W251–W257.
[41] R.S. Liao, R.P. Rennie, J.A. Talbot, Comparative evaluation of a new fluorescent carboxyfluorescein diacetate-modified microdilution method for antifungal susceptibility testing of candida albicans isolates, Antimicrob. Agents Chemother. 46 (10) (2002) 3236–3242.
[42] H.M. Davey, P. Hexley, Red but not dead? Membranes of stressed *Saccharomyces cerevisiae* are permeable to propidium iodide, Environ. Microbiol. 13 (1) (2011) 163–171.
[43] E.L. Steels, R.P. Learmonth, K. Watson, Stress tolerance and membrane lipid unsaturation in *Saccharomyces cerevisiae* grown aerobically or anaerobically, Microbiology 140 (3) (1994) 569–576.
[44] D.J. Jamieson, *Saccharomyces cerevisiae* has distinct adaptive responses to both hydrogen peroxide and menadione, J. Bacteriol. 174 (20) (1992) 6678–6681.
[45] S. Izawa, Y. Inoue, A. Kimura, Importance of catalase in the adaptive response to hydrogen peroxide: analysis of acatalasaemic *Saccharomyces cerevisiae*, Biochem. J. 320 (Pt 1) (1996) 61–67.
[46] E.O. Garrido, C.M. Grant, Role of thioredoxins in the response of *Saccharomyces cerevisiae* to oxidative stress induced by hydroperoxides, Mol. Microbiol. 43 (4) (2002) 993–1003.
[47] A. Sousa-Lopes, F. Antunes, L. Cyrne, H.S. Marinho, Decreased cellular permeability to H2O2 protects *Saccharomyces cerevisiae* cells in stationary phase against oxidative stress, FEBS Lett. 578 (1–2) (2004) 152–156.
[48] A. Ocampo, J. Liu, E.A. Schroeder, G.S. Shadel, A. Barrientos, Mitochondrial respiratory thresholds regulate yeast chronological lifespan and its extension by

caloric restriction, Cell Metab. 16 (1) (2012) 55–67.
[49] D. Carmona-Gutierrez, T. Eisenberg, S. Buttner, C. Meisinger, G. Kroemer, F. Madeo, Apoptosis in yeast: triggers, pathways, subroutines, Cell Death Differ. 17 (5) (2010) 763–773.
[50] M. Reers, T. Smith, L. Chen, J-aggregate formation of a carbocyanine as a quantitative fluorescent indicator of membrane-potential, Biochemistry 30 (1991) 4480–4486.
[51] S.T. Smiley, M. Reers, C. Mottola-Hartshorn, M. Lin, A. Chen, T.W. Smith, et al., Intracellular heterogeneity in mitochondrial membrane potentials revealed by a J-aggregate-forming lipophilic cation JC-1, Proc. Natl. Acad. Sci. 88 (9) (1991) 3671–3675.
[52] F. Madeo, E. Fröhlich, M. Ligr, M. Grey, S.J. Sigrist, D.H. Wolf, et al., Oxygen stress: a regulator of apoptosis in yeast, J. Cell Biol. 145 (4) (1999) 757–767.
[53] M.S. Siskind, C.E. McCoy, A. Chobanian, J.H. Schwartz, Regulation of intracellular calcium by cell pH in vascular smooth muscle cells, Am. J. Physiol. Cell Physiol. 256 (2) (1989) C234.
[54] S. Dorion, A. Clendenning, J. Jeukens, J.J. Salas, N. Parveen, A.A. Haner, et al., A large decrease of cytosolic triosephosphate isomerase in transgenic potato roots affects the distribution of carbon in primary metabolism, Planta 236 (4) (2012) 1177–1190.
[55] M. Coen, S.U. Ruepp, J.C. Lindon, J.K. Nicholson, F. Pognan, E.M. Lenz, et al., Integrated application of transcriptomics and metabonomics yields new insight into the toxicity due to paracetamol in the mouse, J. Pharm. Biomed. Anal. 35 (1) (2004) 93–105.
[56] L. Tretter, V. Adam-Vizi, Alpha-ketoglutarate dehydrogenase: a target and generator of oxidative stress, Philos. Trans. R. Soc. B: Biol. Sci. 360 (1464) (2005) 2335–2345.
[57] P. Dick Tobias, M. Ralser, Metabolic remodeling in times of stress: who shoots faster than his shadow?, Mol. Cell 59 (4) (2015) 519–521.
[58] J.R. Ussher, J.S. Jaswal, G.D. Lopaschuk, Pyridine nucleotide regulation of cardiac intermediary metabolism, Circ. Res. 111 (5) (2012) 628.
[59] A.P. Fernandes, A. Holmgren, Glutaredoxins: glutathione-dependent redox enzymes with functions far beyond a simple thioredoxin backup system, Antioxid. Redox Signal. 6 (1) (2004) 63–74.
[60] A. Holmgren, J. Lu, Thioredoxin and thioredoxin reductase: current research with special reference to human disease, Biochem. Biophys. Res. Commun. 396 (1) (2010) 120–124.
[61] L.E.S. Netto, F. Antunes, The roles of peroxiredoxin and thioredoxin in hydrogen peroxide sensing and in signal transduction, Mol. Cells 39 (1) (2016) 65–71.
[62] H.J. Forman, Redox signaling: an evolution from free radicals to aging, Free Radic. Biol. Med. 97 (2016) 398–407.
[63] W.Y. Kang, S.H. Kim, Y.K. Chae, Stress adaptations of *Saccharomyces cereviseae* as monitored via metabolites using two-dimensional NMR spectroscopy, FEMS Yeast Res. 12 (5) (2012) 608.
[64] I. Vermes, C. Haanen, H. Steffens-Nakken, C. Reutellingsperger, A novel assay for apoptosis Flow cytometric detection of phosphatidylserine expression on early apoptotic cells using fluorescein labelled Annexin V, J. Immunol. Methods 184 (1) (1995) 39–51.
[65] L. Galluzzi, I. Vitale, J.M. Abrams, E.S. Alnemri, E.H. Baehrecke, M.V. Blagosklonny, et al., Molecular definitions of cell death subroutines: recommendations of the Nomenclature Committee on Cell Death 2012, Cell Death Differ. 19 (1) (2012) 107–120.
[66] J. Lu, A. Holmgren, The thioredoxin antioxidant system, Free Radic. Biol. Med. 66 (2014) 75–87.
[67] C.C. Winterbourn, D. Metodiewa, Reactivity of biologically important thiol compounds with superoxide and hydrogen peroxide, Free Radic. Biol. Med. 27 (3–4) (1999) 322–328.